Stabilization of the smectic-C^*_α phase in mixtures with chiral dopants

Hak Sun Chang,[1] Shaden Jaradat,[1] Helen F. Gleeson,[1] Ingo Dierking,[1] and Mikhail A. Osipov[2]
[1]*School of Physics and Astronomy, University of Manchester, Manchester M139PL, United Kingdom*
[2]*Department of Mathematics, University of Strathclyde, 26 Richmond Street, Glasgow G11XH, United Kingdom*
(Received 15 December 2008; published 26 June 2009)

A series of mixtures comprising an antiferroelectric liquid-crystal host and a chiral dopant is described in which the layer spacing variation at the orthogonal smectic-A^* (SmA^*) to tilted smectic-C^* or smectic-C^*_α (SmC^* or SmC^*_α) phase transition changes from the usual strong contraction in the pure system to one in which there is almost no layer spacing change observed across the transition for dopant concentrations of 7%. The nature of the orthogonal to tilted phase transition is examined using Raman spectroscopy, to determine the order parameters $\langle P_2\rangle$ and $\langle P_4\rangle$ in the SmA^* phase, and via a generalized Landau expansion to reveal the details of the phase transition itself. The results show that the value of $\langle P_2\rangle$ at the orthogonal to tilted transition increases from around 0.6 to 0.7 as the dopant concentration increases, while $\langle P_4\rangle$ remains constant at approximately 0.4 irrespective of dopant concentration. Further, the generalized Landau potential measurements prove that the transition is purely second order, while electro-optic measurements confirm that the tilt angle at the transition becomes smaller with increasing dopant concentration. The combined data show that the high-temperature tilted phase regime corresponds to a SmC^*_α phase rather than the mechanism suggested by de Vries that is inferred by the layer spacing data alone. We demonstrate that the lower-temperature SmC^*_α-SmC^* phase transition is of first order. Further, the temperature range of the SmC^*_α phase increases dramatically with concentration, from around 2 K in the pure system to around 21 K in the 8% doped mixture, showing that the chiral dopant plays a role in stabilizing this phase. Indeed, we particularly note that for the 8% doped mixture all other SmC^*-like phases disappear and that the only tilted phase remaining is SmC^*_α. This implies that we are reporting a liquid-crystalline phase sequence, namely, cryst.-SmC^*_α-SmA^*-iso., i.e., a direct transition between the SmC^*_α phase and the crystalline phase.

DOI: 10.1103/PhysRevE.79.061706 PACS number(s): 64.70.M−, 42.70.Df, 61.30.−v

I. INTRODUCTION AND BACKGROUND

Liquid crystals are well-known materials that permeate into our daily life primarily through various display media including calculators, mobile phones, monitors, and televisions [1]. These displays use the *nematic* phase, which exhibits orientational order only, and in which the average direction of the rodlike molecules is defined by the director (**n**). Although nematic liquid-crystal displays have been enormously successful, there has been strong interest in ferroelectric liquid crystals since their discovery some 30 years ago [2], as they offer bistability and electro-optic switching that is up to 3 orders of magnitude faster than that of nematic systems. The most common liquid-crystal state that exhibits ferroelectricity is the chiral smectic-C phase (SmC^*) in which molecules are arranged in layers, with the director inclined to the layer normal by a temperature-dependent tilt angle, θ. The chiral nature of the phase (denoted by the asterisk) is apparent in the helicoidal structure adopted in the bulk of the material in the absence of external fields. The helical pitch is usually of the order of several hundred layers; thus, molecules in adjacent layers essentially point in the same direction (i.e., synclinic ordering). In addition to the smectic-C^* phase, several other chiral tilted phases exist with antiferroelectric or ferrielectric properties [3], which can be distinguished by the characteristic interlayer ordering. In the antiferroelectric SmC^*_A phase, the molecular ordering is anticlinic (two-layer repeat unit). Furthermore, at least two other phases intermediate to the SmC^*_A and SmC^* phases are known to exist: the ferrielectric SmC^*_{FI1} phase and the antiferroelectric SmC^*_{FI2} phase, which have three- and four-layer repeat units, respectively [4–6]. These phases are on occasion also referred to as intermediate phases. Finally, the SmC^*_α phase, which exhibits an incommensurate [7] short helical pitch structure, can occur at temperatures just below the smectic-A^* phase, i.e., the untilted orthogonal smectic phase. It is the SmC^*_α phase, and its stabilization over a much wider temperature range than is usually observed, which are of particular interest in this study.

In discussing the SmC^* phase, it is important to recognize that there is more than one way in which it can form from the SmA^* phase. Specifically, one can envisage a system in which either the (approximately) orthogonal molecules in the SmA^* phase tilt essentially uniformly at the transition or one in which the tilted director results from a condensation of a uniform azimuthal distribution of tilt directions in the SmA^* phase (the *diffuse-cone* configuration [8]). The former is the more common manifestation of the transition to the SmC^* phase, in which the transition is typically accompanied by a significant contraction in layer spacing caused by the molecular tilting, while the latter is often referred to as a *de Vries* material [9] which is currently attracting significant attention because of its potential for devices. This potential comes from a recognition that one of the major barriers to fully commercializing ferroelectric liquid-crystal displays has been the fact that strong layer contraction normally results in a chevron structure [10] and associated zigzag defects, which significantly degrade the device performance. The almost constant layer spacing across the transition from the de Vries-type SmA^* to the SmC^* phase means that nei-

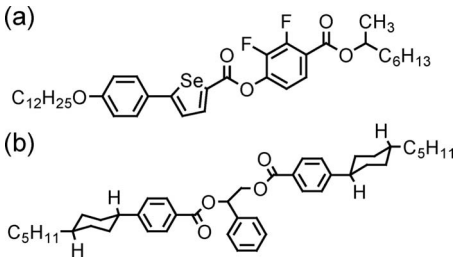

FIG. 1. Molecular structure of (a) the host material AIS179 and (b) the chiral dopant S1011.

ther the chevron nor the zigzag defects form. The de Vries system is further characterized by relatively low orientational order in the SmA^* phase as a result of the azimuthal distribution of the director. It is noteworthy that the SmC^*_α phase is actually almost indistinguishable from the SmC^* phase of a de Vries system in the bulk since the SmC^*_α phase has an extremely tight pitch, which can be considered as a distribution of azimuthal directions of tilt from one layer to another (as is the case in the diffuse-cone description of the SmA^* phase). It important to note that, as has very recently been demonstrated, a nonlayer shrinkage transition can also be obtained by taking into account intralayer interactions [11], allowing systems with low layer shrinkage and relatively high-order parameter.

Understanding and differentiating these systems is important since the nature of the transitions must be distinct and both have technological importance. In this paper, we report a detailed study of a system in which the orthogonal to tilted smectic phase transition shows the low layer shrinkage. By studying a series of mixtures in which we systematically vary the concentration of a chiral dopant, we seek to understand the nature of the underlying phase and phase transitions. In particular, we identify features that result in the stabilization of the SmC^*_α phase in a system that also exhibits the anomalously weak layer contraction usually associated with the de Vries system.

II. MATERIALS AND EXPERIMENTS

The mixtures are composed of two materials with equivalent handedness (sign of chirality). The host material (denoted AIS179) includes a selenophene ring and a fluorine substituted benzene ring in the core [Fig. 1(a)] and has been investigated in detail elsewhere [7,12]. The phase sequence includes the SmA^*, SmC^*_{FI1}, and SmC^*_A phases, confirmed by resonant x-ray scattering, and a SmC^*_α phase that was too narrow ($\sim$1 K wide) to be investigated using that technique. The dopant is the chiral material, S1011 (Merck Ltd) and its molecular structure is shown in Fig. 1(b). The host is doped with the chiral material at concentrations from 1% to 8% (by weight). The intermediate phases of these mixtures have also been studied extensively [6,13]. These systems, and those in a sister system [14] in which the host does not include the fluorination, exhibit remarkably wide intermediate phases, up to 30 K in temperature range. This paper, however, is concerned with the temperature range in the vicinity of the orthogonal to tilted smectic transitions.

The SmC^*_α phase is difficult to differentiate from the SmC^* phase. Although both phases have the same symmetry, it is clear that there are distinct thermodynamic phase transitions between them [15]. The most reliable and straightforward indicator of the SmC^*_α phase is the current response to an applied triangular electric field [16] which shows two polarization reversal peaks (analogous to an antiferroelectric system), one of which grows with decreasing temperature, while the other peak decreases, implying ferrielectriclike characteristics. On further decreasing the temperature, the two asymmetric current peaks merge into a single ferroelectriclike peak. Examining the current response therefore offers a method to determine the range of the SmC^*_α phase.

In order to fully characterize the systems, we obtained information on the smectic layer spacing and the orientational order parameters as functions of temperature, in addition to examining the phase transitions by deducing the Landau coefficients. The layer spacing of the mixtures was measured across the range of all the liquid-crystal phases via small-angle x-ray scattering (SAXS). The samples were held in a Linkam hot stage identical to that used for all other measurements reported in this paper, providing a relative accuracy of ± 0.1 K. The experiments were carried out at station 2.1 of the Synchrotron Radiation Source, Daresbury, UK using an incident wavelength of 1.54 Å and a camera length of 1 m, allowing the layer spacing to be deduced with an accuracy of ± 0.05 Å.

The orientational order parameters, $\langle P_2 \rangle$ and $\langle P_4 \rangle$ were measured across the SmA^* phase via polarized Raman spectroscopy (PRS) using a method recently shown to give excellent results in the nematic phase of 4-cyano-4′-octylbiphenyl (8CB) [17]. A Renishaw 1000 Raman microscope was used for the measurements, operating with an Ar^+ laser emitting light of wavelength 514 nm with a power of 10 mW. For the Raman measurements, devices of 12 μm gap thickness were constructed using 150-μm-thick glass substrates, with rubbed alignment layers to promote excellent planar alignment of the liquid crystals. The thicker liquid-crystal samples and thinner glass improve the Raman signal, allowing more accurate measurement of the order parameters. All the samples had two strong Raman-active bands corresponding to a symmetric stretching of the benzene rings (1605 cm^{-1}) and the selenophene ring (1444 cm^{-1}) [18], as well as several weaker bands, as seen in the typical spectrum shown in Fig. 2. The two main peaks described above are strongly polarized along the molecular long axis and are suitable probes for the order-parameter measurements.

The backscattered Raman peak intensities were measured with the analyzer set to select the intensity perpendicular ($I_\perp$) or parallel ($I_\parallel$) to the incident polarization over a 360° rotation of the sample in 10° steps. This allowed the depolarization ratio ($I_\perp / I_\parallel$) to be obtained and a fit to the depolarization ratio curve yields the order parameters $\langle P_2 \rangle$ and $\langle P_4 \rangle$ [17] with an accuracy of approximately 10%.

In order to determine the Landau coefficients, both the total polarization and the tilt angle of the materials need to be determined as a function of applied electric ac field and temperature across the phase transitions. For these electro-optic measurements the liquid-crystalline materials were contained

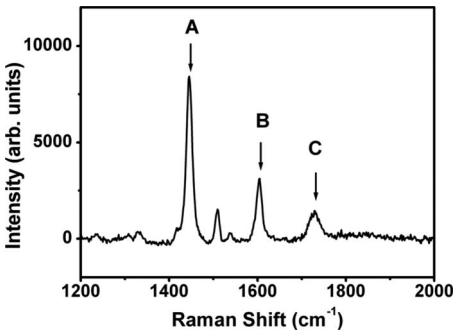

FIG. 2. Typical Raman spectrum of the 7% doped mixture. Two intense peaks can be seen at (A) 1444 cm^{-1} and (B) 1605 cm^{-1}, corresponding to the symmetric stretching of the benzene rings and the selenophene ring, respectively. The third peak, (C), at 1729 cm^{-1} is associated with carbonyl stretching.

in devices of nominal thickness 2 μm with transparent indium-tin oxide (ITO) electrodes to enable the application of electric fields across the sample. The cells employed (AWAT PPW, Poland) had unidirectionally rubbed polyimide on one substrate, while the second substrate was unrubbed. The optical tilt angle and total polarization of the materials were measured as functions of applied ac electric field and temperature using established techniques by Bahr and Heppke [19] and the well-known triangular wave method [20], respectively. Both measurements provided input to the generalized Landau model [21], allowing parameters associated with the phase transition to be deduced, as described below. The tilt angle θ was measured with an accuracy of $\pm 0.1°$, while the total polarization P was obtained with an accuracy of 1% after subtracting the ohmic current contribution. The generalized Landau model [21] gives the change in the Gibbs free energy as

$$g - g_0 = \frac{1}{2}\alpha(T - T_C)\theta^2 + \frac{1}{4}b\theta^4 + \frac{1}{6}c\theta^6 + \frac{1}{2\chi_0\varepsilon_0}P^2 - CP\theta - \frac{\Omega P^2\theta^2}{2} - PE, \quad (1)$$

where α, b, and c are the Landau coefficients, T_C is the transition temperature of the achiral material, χ_0 is the dielectric susceptibility at high frequencies, C is the bilinear coupling coefficient, and Ω is the biquadratic polarization-tilt coupling coefficient. When the free-energy density of Eq. (1) is minimized with respect to P, the polarization is given by [22]

$$P = \frac{C\theta + E}{\frac{1}{\varepsilon_0\chi_0} - \Omega\theta^2}. \quad (2)$$

From a graph of $P(\theta)$ the three coefficients C, χ_0, and Ω are obtained by a multicurve fitting procedure which uses tilt angle and polarization at different applied electric field amplitudes. Resubstitution of Eq. (2) into Eq. (1) and minimization with respect to θ gives [22]

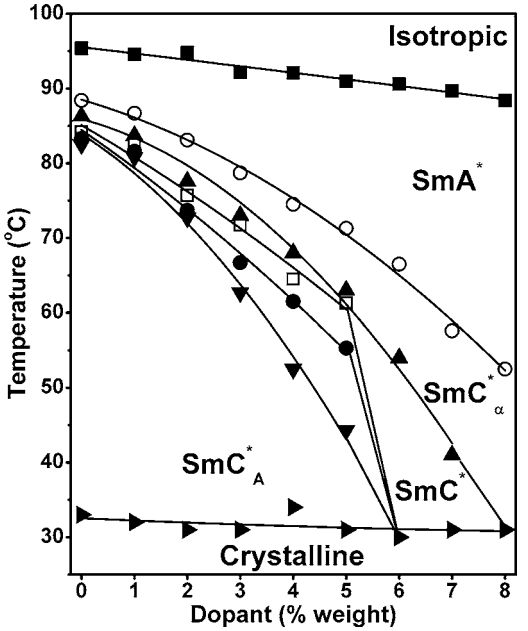

FIG. 3. Phase diagram of the mixtures with chiral dopants. Note that at high concentrations above 7% a phase sequence of cryst-SmC^*_α-SmA^*-iso is observed. (■: isotropic-SmA^*, ○: SmA^*-SmC^*_α, ▲: SmC^*_α-SmC^*, □: SmC^*-SmC^*_{FI2}, ●: SmC^*_{FI2}-SmC^*_{FI1}, ▼: SmC^*_{FI1}-SmC^*_A, and ▶: SmC^*_A-crystalline phase transition)

$$T(\theta,E) = T_C - \frac{1}{\alpha}\left[b\theta^2 + c\theta^4 - \frac{(C\theta + E)\left(\frac{C}{\varepsilon_0\chi_0} + \Omega\theta E\right)}{\theta\left(\frac{1}{\varepsilon_0\chi_0} - \Omega\theta^2\right)^2} \right]. \quad (3)$$

Because the three coefficients C, χ_0, and Ω are already known, the remaining parameters α, b, c, and T_C in Eq. (3) can be determined from the temperature dependence of the tilt angle at different applied electric fields. In order to obtain the Landau coefficients the procedure described was applied to data for the temperature range of both the SmA^* to SmC^*_α and SmC^*_α to SmC^* transitions with the phase boundaries determined separately through observation of the current pulse response.

III. RESULTS AND DISCUSSIONS

The phase diagram of the system (Fig. 3) has been determined via polarized microscopy, x-ray scattering, and observation of electro-optic responses. Specifically, the phase diagram close to the orthogonal/tilted transition has been determined by using the current reversal method described above to distinguish between the SmC^* and SmC^*_α phases. It is noteworthy that increasing concentrations of the chiral dopant enhances the stability of the intermediate phases at low concentrations (described elsewhere [6]) and the SmC^*_α phase over a wider concentration range. This stabilization is remarkable; the SmC^*_α phase is stable over a temperature range of 16 K in the 7% mixture compared to only 2 K for

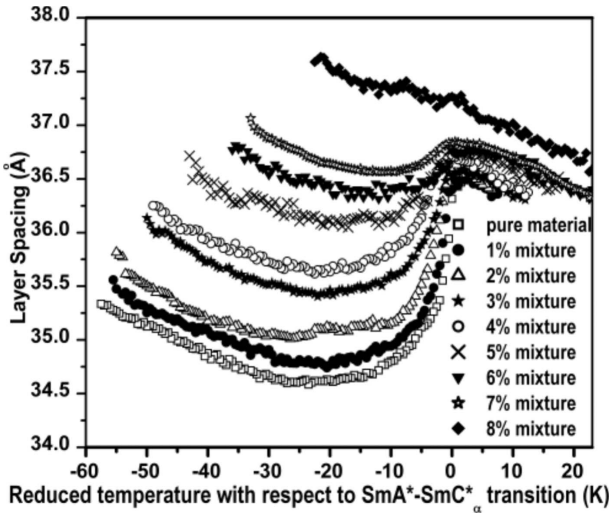

FIG. 4. Layer spacing of the mixtures as a function of reduced temperature, the temperature where the orthogonal to tilted transition occurs.

the pure material. For the 8% mixture the stability regime of the SmC^*_α phase increases even further to about 20 K, but more importantly, we note that all other tilted SmC^*-like phases have vanished at this concentration, including the antiferroelectric, intermediate (ferrielectric), and the ferroelectric phases. We thus observe the phase sequence of cryst-SmC^*_α-SmA^*-iso, i.e., a direct transition between the crystalline and the SmC^*_α phase.

The stability of the SmA^* phase is also increased in the highly doped mixtures, an indirect indication that the smectic order has increased (a factor known to stabilize the SmC^*_α phase [23]). Furthermore, the stabilization of the SmC^*_α phase with increasing chirality is in good agreement with the theory by Cepic *et al.* [24] although the probable origin of the SmC^*_α phase is the frustration between the nearest and next-nearest layer interaction [25].

We now consider the layer spacing of the materials as a function of temperature and dopant concentration, shown in Fig. 4. Several features are apparent, which are similar to those already reported for a similar mixture set [14]. First, note that the layer spacing in the SmA^* phase (above a reduced temperature of 0 K on the graph) increases with increasing dopant concentration by approximately 0.3 Å (almost 1%) over 15 K in mixtures with sufficiently wide SmA^* temperature range.

There is a strong almost linear expansion of the layers with reduced temperature for all of the mixtures which accounts for the larger layer spacing in the low-temperature regime. We are especially interested in the region around the orthogonal to tilted transition where it is observed that the layer contraction changes from strong (~5%) at low dopant concentrations (full circles) to anomalously weak (~0.8%) at higher concentrations (open stars). Indeed, for the 7% mixture, the contraction is about 1 order of magnitude lower than that observed for the pure system, while for the 8% mixture a smectic layer contraction is practically absent. It is noteworthy that typical de Vries materials are reported to exhibit a layer shrinkage of approximately 1% [26]. The key

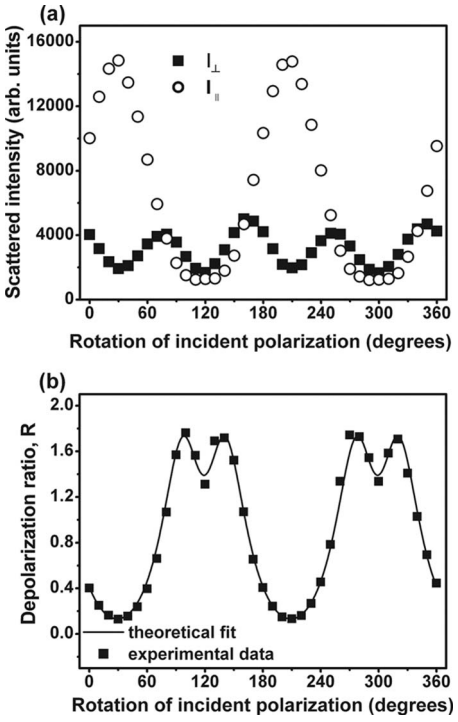

FIG. 5. (a) Polarized Raman scattered intensities $I_\perp$ and $I_\parallel$ at 90 °C obtained in the pure host material for all orientations of the planar sample. (b) Corresponding experimental depolarization ratio profile (squares) and the fitted theoretical profile (line).

observation for the purpose of this work is that, with increasing dopant concentration, the orthogonal to tilted phase transition becomes less and less characterized by strong layer contraction. In several other materials such a feature has been associated with a de Vries-type behavior based on the diffuse-cone arrangement in the SmA^* phase.

Raman spectroscopy allows the order parameters in the SmA^* phase to be readily determined, thus enabling one to potentially distinguish between a conventional orthogonal to tilted phase transition or a de Vries-type transition. Figure 5(a) shows two exemplary experimental Raman scattered intensities, $I_\perp$ and $I_\parallel$ determined for the pure material at a temperature of 90 °C (5 °C below the SmA^* to isotropic phase transition). The corresponding depolarization ratio, $R = I_\perp / I_\parallel$, can be calculated from these data and is shown in Fig. 5(b). The fitted depolarization ratio profile is shown as the solid line, which is in excellent agreement with the experimental data. Similar data are obtained for all mixtures across the SmA^* phase regimes.

Figure 6 shows the measured values of $\langle P_2 \rangle$ and $\langle P_4 \rangle$ deduced by the fitting method applied to the whole angular depolarization ratio profile [27]. Comparing the order parameters as a function of reduced temperature for each mixture, it can be seen that both $\langle P_2 \rangle$ and $\langle P_4 \rangle$ increase and become saturated with decreasing temperature as expected. It can also be seen that the order parameters are essentially equivalent for each mixture. Furthermore, the maximum value of $\langle P_4 \rangle$ is approximately 0.4, which is much larger than is obtained for the SmA^* phase in a typical de Vries system [28] and consistent with a conventional SmA^* phase. Thus, it seems unlikely that this large value of the order parameter is

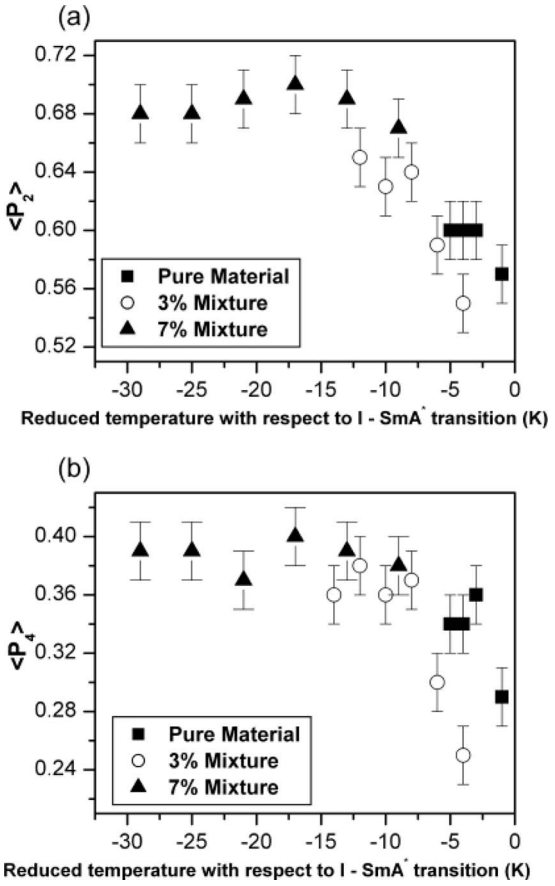

FIG. 6. Dependence of the order parameters (a) $\langle P_2 \rangle$ and (b) $\langle P_4 \rangle$ as functions of reduced temperature (where the temperature is measured with respect to the I-SmA^* transition temperature) for selected mixtures. Data for other mixtures fit the trends indicated.

associated with a de Vries system even though there is hardly any layer contraction in the high-concentration mixtures.

The nature of the phase transitions as a function of dopant concentration can be deduced from the generalized Landau model. Typical data illustrating the employed method of parameter determination by the generalized Landau model are shown in Fig. 7. Since there are two phase transitions involving the SmC^*_α phase, the temperature range is divided into two regimes around the SmA^*-SmC^*_α and the SmC^*_α-SmC^* phase transitions. The temperature range of Figs. 7(a) and 7(b) is that across the SmA^* and SmC^*_α transition. The former shows total polarization P versus tilt angle θ and the latter illustrates the temperature dependence of the tilt angle at various applied electric fields. Equivalent data are shown in Figs. 7(c) and 7(d) for the SmC^*_α to SmC^* transition. Four different electric fields were applied above the value required to unwind the helical superstructure completely.

As can be seen in Fig. 7(a), experimental data are well fitted by Eq. (2) using one-parameter set consisting of C, χ_0, and Ω. The coefficient C is the only chirality-related parameter and is given by the initial slope, $dP/d\theta$, at small tilt angles. The coefficient Ω describes the deviation from the linear polarization-tilt coupling at large tilt angles. The coefficient χ_0 is proportional to the change in polarization with respect to the applied electric field. These three coefficients

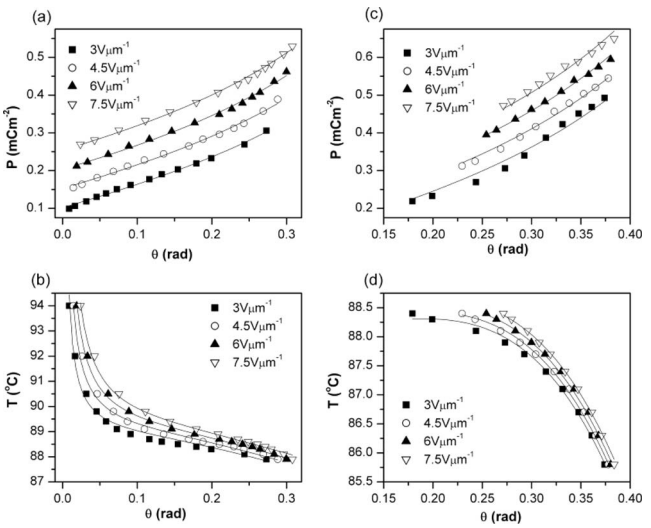

FIG. 7. Typical examples demonstrating parameter determination using the generalized Landau model. The data show (a) tilt-polarization coupling [the symbols are experimental data and the solid lines are simultaneous best fits to Eq. (2)] of the host material at various electric field amplitudes and (b) temperature dependence of the tilt angle [the solid lines are simultaneous best fits to Eq. (3)] for the SmA^*-SmC^*_α phase transition. Data from similar measurements to those shown in (a) and (b) for the SmC^*_α-SmC^* phase transition are presented in (c) and (d), respectively.

(C, χ_0, Ω) can now be fixed in Eq. (3) to determine the Landau coefficients α, b, and c, as well as T_C by simultaneously fitting all data depicted in Fig. 7(b). Again, an excellent fit can be obtained for all materials investigated. In Figs. 7(c) and 7(d) the same method was applied for the SmC^*_α to SmC^* transition. Only one data set is shown for reasons of clarity, and equally good fits were obtained for all samples investigated.

Figure 8 summarizes the dependence of all parameters on dopant concentration for the SmA^* to SmC^*_α (0–8 % dopant, triangles) and the SmC^*_α to SmC^* (0–7 % dopant, circles) transitions. The chiral bilinear (piezoelectric) coupling term C increases linearly with increasing dopant concentration for both transitions [Fig. 8(a)]. The increase in the coefficient C is directly related to chirality, confirming that the chiral dopant increases the chirality of the mixtures. This can be interpreted as an important reason for the stabilization of the SmC^*_α phase [24]. The dielectric susceptibility at high frequencies, χ_0, remains practically constant [Fig. 8(b)], which implies that the addition of the dopant does not change the molecular polarizability to any significant extent, as expected. The biquadratic coupling constant, Ω, related to the quadrupolar order of the system, tends to decrease slightly for the highly doped mixtures [Fig. 8(c)]. The biquadratic coupling constant is one of the parameters that are determined with the lowest accuracy (an error of approximately 25%). Within this experimental error Ω appears to decrease with increasing dopant concentration, but no functionality can be deduced. The first Landau coefficient α decreases with increasing dopant concentration across both the SmA^*-SmC^*_α and the SmC^*_α-SmC^* transitions [Fig. 8(d)].

The decrease in the α coefficient implies an increase in the electroclinic effect. This decrease in α by approximately

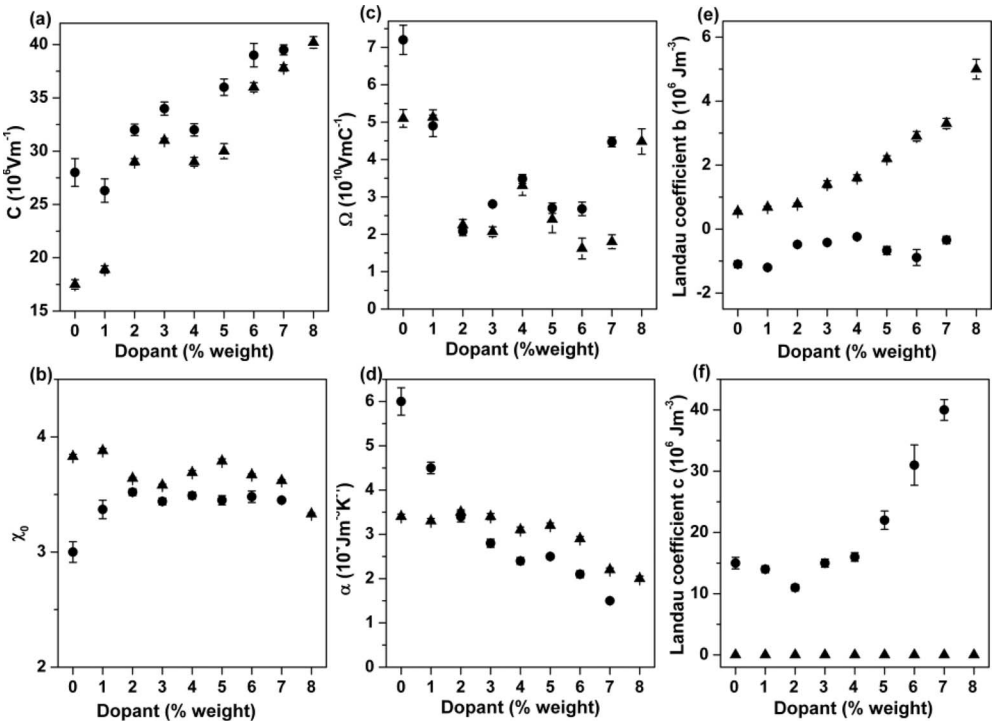

FIG. 8. Parameters of the generalized Landau model as functions of dopant concentration for the SmA^*-SmC^*_α phase transition (triangles) and the SmC^*_α-SmC^* phase transition (circles): (a) bilinear (piezoelectric) coupling coefficient C; (b) dielectric constant at high frequencies χ_0; (c) biquadratic polarization-tilt coupling coefficient Ω; (d) first Landau coefficient α; (e) second Landau coefficient b; and (f) third Landau coefficient c.

a factor of 2 is not nearly as pronounced as is observed for de Vries systems, where α is generally smaller by a factor of 5 or more in comparison to standard materials [22,29]. The second Landau coefficient b, which is related to the order of the phase transition ($b>0$ for a second order and <0 for a first-order transition), has quite different tendencies for the SmA^*-SmC^*_α and the SmC^*_α-SmC^* transition [Fig. 8(e)].

The b coefficient has a positive value and increases with increasing dopant concentration for the SmA^*-SmC^*_α transition, indicating a strongly second-order phase transition, contrary to the SmC^*_α-SmC^* phase transition where the coefficient b has a negative value for all dopant concentrations, indicating a transition of first order. In this system, the third Landau coefficient, c, is always found to be very close to zero, taking either positive or negative values. There is always a relatively large error ($\sim$25%) associated with this parameter. As theoretical description does not need this term, we have therefore chosen to set it to zero for the SmA^*-SmC^*_α transition in this system [Fig. 8(f)]. In contrast, the c-coefficient values for the SmC^*_α-SmC^* transition exhibit values of similar magnitude to these observed in other investigations [30]. Furthermore, the c-coefficient is found to increase with increasing dopant concentration, indicating a steepening of the potential for large tilt angles at dopant concentrations larger than approximately 4%.

It is interesting to consider further the difference in the coefficients of the free-energy expansion in the SmC^* and SmC^*_α phase. In particular, the experimentally determined sign of the coefficient b is negative in the SmC^* phase and positive in the SmC^*_α phase, respectively. This means that without the SmC^*_α phase the SmC^*-SmA^* phase transition would be of first order, while the actual SmC^*_α-SmA^* transition is of second order. This difference can qualitatively be explained by the existence of the helical superstructure with a very short pitch in the SmC^*_α phase.

One may wonder why the coefficients of the free-energy expansion appear to be different in the SmC^* and SmC^*_α phases, as shown experimentally in this work. The answer to this question is related to the difference between the two tilted phases. It is well known that the symmetry of the SmC^* and the SmC^*_α phase is indeed the same but the existence of the normally distinct first-order phase transition between them indicates that in our case an abrupt change in the helical structure appears to be very important. (It is worthwhile pointing out though that the transition can also resemble second-order behavior when approaching the critical point, i.e., a continuous evolution of the pitch across the SmC^*_α-SmC^* transition, similar to the density at the critical point of the liquid-gas transition.) One notes that the SmA^*-SmC^*_α transition is the tilting transition with the tilt angle θ being the primary order parameter in this case. In contrast, the SmC^*-SmC^*_α transition is a transition between two tilted phases which possess the same symmetry. Thus there is no symmetry change at the transition, and the transition resembles the gas-liquid transition, which is characterized by a large change in density (which nevertheless is nonzero in both phases). In the case of the SmC^*-SmC^*_α transition the role of density is taken on by the pitch p of the helical superstructure which is the scalar order parameter for this transition.

In the general case the free energy of the SmC^* and the SmC^*_α phases depends on both the tilt angle and the pitch (or the wave vector q of the helical structure which is proportional to the inverse pitch $1/p$). However, in the SmC^* phase the pitch is large (several hundred nanometers to micrometers) and the corresponding contribution is known to be small and can be neglected. On the other hand, in the SmC^*_α phase the pitch is very small (of order ten nanometer), and the contribution to the free energy associated with the helical superstructure may be significant. One notes that the tilt angle is sufficiently small throughout the SmC^*_α phase and also in the vicinity of the SmC^*-SmC^*_α transition that the free energy may be expanded in powers of the tilt angle (which justifies the experimental approach used in this paper). Moreover, even in the SmC^*_α phase the pitch is several times longer than the smectic layer period and can be as large as 20 layers close to the transition into the SmC^* phase [7,31]. Thus one can still obtain qualitative results expanding the free energy also in terms of the wave vector q of the helical structure. Now one notes, that if the free energy of the SmC^*_α phase is first minimized with respect to the wave vector q and then the equilibrium q is substituted back into the total free energy, the resulting energy not only depends on the tilt angle, but the coefficients of the expansion are renormalized. This explicitly explains why the coefficients of the Landau tilt angle expansion corresponding to the total free energy are expected to be different in the two phases, SmC^* and SmC^*_α.

The free energy of the SmC^*_α phase can then be expressed as

$$\Delta G_C = G_0(\Theta, P) + \frac{1}{2}Kq^2 + \Lambda q, \tag{4}$$

where G_0 (θ, P) is the part of the free energy which only depends on the tilt and the spontaneous polarization. This part of the free energy of the tilted phase is given by the general expansion used in the previous sections. In Eq. (4), the parameter K is the twist elastic constant of the tilted phase and Λ is the chiral parameter which has the meaning of the helical twisting power. Minimizing Eq. (4) with respect to q and substituting back into Eq. (4) one obtains

$$\Delta G_C = G_0(\Theta, P) - \frac{1}{2}\frac{\Lambda^2}{K} \tag{5}$$

(i.e., the helical structure gives a negative contribution to the total free energy and thus stabilizes the phase).

The dependence of K and Λ on the tilt angle θ can be determined using the simple discrete model of the smectic-C phase. According to [32], K and Λ are given by

$$K = \Theta^2 d^2 \frac{1}{2}\left[\frac{1}{2}\Delta + B\Theta^2 - \chi C c_f\right] \tag{6}$$

and

$$\Lambda = \Theta^2[\lambda - \chi C], \tag{7}$$

where $\Delta = \Delta_0 (T - T_{ac})$ is the linear coupling coefficient between neighboring smectic layers which vanishes at the synclinic-anticlinic transition point. (T_{ac} is the ferroelectric SmC^* to antiferroelectric SmC^*_A transition temperature). In Eq. (6) B is the so-called biquadratic coupling coefficient between neighboring layers (not to be confused with the second Landau coefficient), χ is the dielectric polarizability of a smectic layer, c_f is the flexoelectric coefficient, and C is the piezoelectric coefficient which couples tilt and polarization, and which has been determined experimentally in this paper for different concentrations of the chiral dopant [Fig. 8(a)]. We stress that the above description does not imply a temperature dependence of the general Landau expansion coefficients α, b, or c. Finally λ is the helical twisting coefficient in the absence of the spontaneous polarization. The wave vector of the helical structure is $q = \Lambda / K$. One notes that the large values of q in the SmC^*_α phase are determined by the abnormally small values of the elastic constant K. According to Eq. (6) the elastic constant K may be small due to the negative flexoelectric contribution $-\chi C c_f$ provided the two positive contributions are small.

The term $\Delta = \Delta_0 (T - T_{ac})/2$ may be small if the system is not too far from the synclinic-anticlinic transition where T is relatively close to T_{ac}. The quadrupolar term $B\theta^2$ may be small at small tilt angles. This explains why the SmC^*_α phase is observed only at very small tilt directly below the SmA^*-SmC^* transitions and only in materials which also exhibit the anticlinic phase.

Substituting Eqs. (6) and (7) into Eq. (5) one obtains

$$\Delta G_C = G_0(\Theta, P) - \frac{(\lambda - C\chi)^2 \Theta^2}{\Delta_0 (T - T_{ac})/2 + B\Theta^2 - \chi C c_f}. \tag{8}$$

Equation (8) can be expanded in powers of θ, keeping the first two terms of the expansion

$$\Delta G_C = G_0(\Theta, P) - \frac{(\lambda - C\chi)^2}{\Delta_0 (T - T_{ac})/2 - \chi C c_f}\Theta^2 + \frac{B(\lambda - C\chi)^2}{[\Delta_0 (T - T_{ac})/2 - \chi C c_f]^2}\Theta^4 + \cdots. \tag{9}$$

One notes that according to Eq. (9) the helical structure yields a positive contribution to the total coefficient b in the θ^4 term. This contribution may be sufficiently large in the SmC^*_α phase where the elastic constant K, and thus the denominator in Eq. (9) are very small. In contrast, in the SmC^* phase the pitch is large and the last two terms in Eq. (9) give a negligible contribution. According to our experimental data the Landau coefficient b is negative in the SmC^* phase. In the SmC^*_α phase, however, the coefficient b may become positive if the last term in Eq. (9) is sufficiently large. This explains the positive value of b as determined experimentally in the SmC^*_α phase in contrast to the negative value of b in the SmC^* phase. Equation (9) can also be used to explain the increasing stability of the SmC^*_α phase. Indeed, the second term in Eq. (9), which is proportional to θ^2, is negative, and thus it leads to a relative increase in the transition temperature from the SmC^*_α to SmA^* phase. Relative in this context means that the SmC^*_α-SmA^* transition temperature for the chiral doped systems is higher than would be expected by purely doping with the racemate. (Of course all absolute transition temperatures are still lower than those of the pure nondoped material, as would be expected from thermody-

namics). As a result the temperature range of the SmC^*_α phase is increased. The corresponding term in Eq. (9) is proportional to the square of the chirality parameter (λ-$C\chi$) which is expected to grow with the increasing concentration of strongly chiral dopant. According to our experimental data the coefficient C is indeed increasing with increasing dopant concentration [Fig. 8(a)], and one may expect the same from the coefficient λ. Thus the temperature range of the SmC^*_α phase should increase with increasing dopant concentration in agreement with the experiment. Finally, it should be noted that the present simple phenomenological theory cannot be used to interpret the experimentally observed dependence of the Landau coefficients on the dopant concentration because the corresponding variation in the parameters is unknown. We expect the chiral coefficients to increase with increasing dopant concentration, while the synclinic-anticlinic transition temperature, T_{ac}, is decreasing according to our phase diagram. At the same time the variation in the parameters B and Δ_0 is unknown.

IV. CONCLUSION

We have investigated a series of mixtures exhibiting various ferroelectric, ferrielectric, and antiferroelectric liquid-crystal phases. Special attention was devoted to the regime where the SmA^*-SmC^*_α-SmC^* transitions were observed, in order to elucidate the still enigmatic SmC^*_α phase and its phase transitions. From small angle x-ray scattering the temperature dependencies of the smectic layer spacing suggests a decreasing layer contraction in the SmC^* phase with increasing dopant concentration. Such behavior has often been associated with de Vries materials and attributed to the diffuse-cone model. However, we have determined that there is a SmC^*_α phase of increasing stability between the SmA^* and SmC^* phases for increasing dopant concentration as verified by electro-optic experiments. Polarized Raman spectroscopy was employed to determine the $\langle P_2 \rangle$ and $\langle P_4 \rangle$ order parameters, which are relatively large for all mixtures under investigation, confirming that despite the decreasing layer shrinkage, the phase is not deVries-type. Further evidence is presented through determination of the complete Landau potential, which shows α coefficients which are not as small as generally observed for de Vries materials. Thus, although the smectic layer spacing x-ray data alone may thus suggest a deVries-type transition from the SmA^* to the SmC^* phases, in this system the transition is rather via a SmC^*_α phase. Detailed Landau expansion investigations show that the SmA^*-SmC^*_α transition is of second order, while the lower-temperature SmC^*_α-SmC^* transition is of first order. The findings presented here are consistent with a recent theoretical description of systems that exhibit anomalous layer contraction [11]. In the molecular model intralayer interactions are taken into account to successfully reproduce both conventional and anomalously weak layer contraction. This is done by varying the model parameters while the orientational distribution function is qualitatively the same for both cases. Finally, we draw attention to the fact that at rather high chiral dopant concentrations above approximately 7% all antiferroelectric intermediate and ferroelectric phase behavior vanishes with increasing dopant concentration, and we report a phase sequence of cryst-SmC^*_α-SmA^*-iso.

ACKNOWLEDGMENTS

We are grateful to J. W. Goodby, M. Hird, and Merck for supplying liquid crystals and dopants. Financial support from Samsung Electronics Co. is acknowledged.

[1] E. Lueder, *Liquid Crystal Displays* (Wiley-SID, Weinheim, 2001).
[2] R. B. Meyer, L. Liebert, L. Strzelecki, and P. Keller, J. Phys. (Paris), Lett. **36**, L69 (1975).
[3] I. Musevic, R. Blinc, and B. Zeks, *The Physics of Ferroelectric and Antiferroelectric Liquid Crystals* (World Scientific, Singapore, 2000).
[4] P. Mach, R. Pindak, A.-M. Levelut, P. Barois, H. T. Nguyen, C. C. Huang, and L. Furenlid, Phys. Rev. Lett. **81**, 1015 (1998).
[5] A. Cady, J. A. Pitney, R. Pindak, L. S. Matkin, S. J. Watson, H. F. Gleeson, P. Cluzeau, P. Barois, A.-M. Levelut, W. Caliebe, J. W. Goodby, M. Hird, and C. C. Huang, Phys. Rev. E **64**, 050702(R) (2001).
[6] N. W. Roberts, S. Jaradat, M. Thurlow, L. Hirst, Y. Wang, S. T. Wang, Z. Liu, C. C. Huang, B. Jaiming, R. Pindak, and H. F. Gleeson, Europhys. Lett. **72**, 976 (2005).
[7] L. S. Hirst, S. J. Watson, H. F. Gleeson, P. Cluzeau, P. Barois, R. Pindak, J. Pitney, A. Cady, P. Johnson, C. C. Huang, A.-M. Levelut, G. Srajer, J. Pollmann, W. Caleibe, A. Seed, M. R. Herbert, J. W. Goodby, and M. Hird, Phys. Rev. E **65**, 041705 (2002).
[8] A. de Vries, J. Chem. Phys. **71**, 25 (1979).
[9] A. de Vries, Mol. Cryst. Liq. Cryst. Lett. **41**, 27 (1977).
[10] T. P. Rieker, N. A. Clark, G. S. Smith, D. S. Parmar, E. B. Sirota, and C. R. Safinya, Phys. Rev. Lett. **59**, 2658 (1987).
[11] M. A. Osipov, M. A. Gorkunov, H. F. Gleeson, and S. Jaradat, Eur. Phys. J. E **26**, 395 (2008).
[12] L. S. Matkin, H. F. Gleeson, P. Mach, C. C. Huang, R. Pindak, G. Srajer, J. W. Goodby, M. Hird, and A. Seed, Appl. Phys. Lett. **76**, 1863 (2000).
[13] P. Brimicombe, S. Jaradat, N. Roberts, C. Southern, R. Pindak, S. T. Wang, C. C. Huang, and H. F. Gleeson, Eur. Phys. J. E **23**, 281 (2007).
[14] S. Jaradat, N. W. Roberts, Y. Wang, L. S. Hirst, and H. F. Gleeson, J. Mater. Chem. **16**, 3753 (2006).
[15] Z. Q. Liu, S. T. Wang, B. K. McCoy, A. Cady, R. Pindak, W. Caliebe, K. Takekoshi, K. Ema, H. T. Nguyen, and C. C. Huang, Phys. Rev. E **74**, 030702(R) (2006).
[16] Y. Takanishi, K. Hiraoka, V. K. Agrawal, H. Takezoe, A. Fukuda, and M. Matsushita, Jpn. J. Appl. Phys., Part 1 **30**, 2023 (1991).
[17] C. D. Southern and H. F. Gleeson, Eur. Phys. J. E **24**, 119 (2007).
[18] V. Peulon, G. Barbey, and J.-J. Malandain, Synth. Met. **82**,

111 (1996).
[19] C. Bahr and G. Heppke, Liq. Cryst. **2**, 825 (1987).
[20] K. Miyasato, S. Abe, H. Takezoe, A. Fukuda, and E. Kuze, Jpn. J. Appl. Phys., Part 2 **22**, L661 (1983).
[21] B. Zeks, Mol. Cryst. Liq. Cryst. **114**, 259 (1984).
[22] F. Giesselmann, A. Heimann, and P. Zugenmaier, Ferroelectrics **200**, 237 (1997).
[23] A. Fukuda, Y. Takanishi, T. Isozaki, K. Ishikawa, and H. Takezoe, J. Mater. Chem. **4**, 997 (1994).
[24] M. Cepic and B. Zeks, Phys. Rev. Lett. **87**, 085501 (2001).
[25] N. Vaupotic and M. Cepic, Phys. Rev. E **71**, 041701 (2005).
[26] J. P. F. Lagerwall and F. Giesselmann, ChemPhysChem **7**, 20 (2006).
[27] W. J. Jones, D. K. Thomas, D. W. Thomas, and G. Williams, J. Mol. Struct. **614**, 75 (2002).
[28] N. Hayashi, T. Kato, A. Fukuda, J. K. Vij, Y. P. Panarin, J. Naciri, R. Shashidhar, S. Kawada, and S. Kondoh, Phys. Rev. E **71**, 041705 (2005).
[29] U. Manna, J. K. Song, Y. P. Panarin, A. Fukuda, and J. K. Vij, Phys. Rev. E **77**, 041707 (2008).
[30] P. Archer and I. Dierking, Phys. Rev. E **72**, 041713 (2005).
[31] B. K. McCoy, Z. Q. Liu, S. T. Wang, R. Pindak, K. Takekoshi, K. Ema, A. Seed, and C. C. Huang, Phys. Rev. E **75**, 051706 (2007).
[32] J. P. F. Lagerwall, F. Giesselmann, and M. A. Osipov, Liq. Cryst. **33**, 625 (2006).